Inverse-Polar Ray Projection for Recovering Projective Transformations

Yun Zhang
The Center for Advanced Computer Studies
University of Louisiana at Lafayette
yxz2646@louisiana.edu

Henry Chu
The Center for Advanced Computer Studies
University of Louisiana at Lafayette
cice@cacs.louisiana.edu

Abstract

A ray projection in the inverse-polar space is proposed for recovering a projective transformation between two segmented images. The images are converted from their original Cartesian space to the inverse-polar space. Then, the two ray projections—one shift-invariant and the other shift-sensitive—of the inverse-polar images are computed to create two sets of data. Based on the obtained projection data, a two-step strategy is employed to recover the projective transformation. In the first step, the shift-invariant data are used to recover the four affine parameters. In the second step, the shift-sensitive data are used to recover the two projective parameters. The remaining two translation-related parameters are recovered in, e.g., an exhaustive search combined with the two-step recovery strategy. The proposed approach has been tested successfully to recover a variety of projective transformations between real images.

1. Introduction

The recovery of projective transformations from images taken from different viewpoints is an essential task in computer vision. Methods such as the stratified reconstruction rely on assumptions of the scene and features extracted from the images. An alternative approach is to extract the projective transformation parameters from the contour of imaged regions (or objects). Based on the concept of integral geometry [9], the trace transform [4], a generalization of the Radon transform [2, p. 505], has been proposed. It was successfully applied to recovering similarity or affine transformations between segmented images [4, 5]. Practical techniques for evaluating shift-invariant or shift-sensitive one-dimensional (1-D) functions have also been developed [4, 5, 10]. We extend these techniques in the present work for recovering projective transformations.

In this paper, a ray projection in the inverse-polar space, termed *inverse-polar ray projection*, is proposed to solve the problem of recovering a projective transformation between two segmented images. The proposed recovering process makes use of information about the shape and appearance of an imaged object. In particular, three key contributions are made. First, the inverse-polar transform, which was recently introduced for recovering the two projective parameters [11], is extended as a mathematical tool for recovering a complete projective transformation. Secondly, a ray projection, a generalization of the fan-beam projection [6, p. 92], is proposed as a workhorse to produce data that are used to determine the transformation. Finally, a feasible two-step strategy for the recovering is established.

The proposed inverse-polar ray projection has its unique features. This can be clarified by a comparison between the recently introduced 1-D mappings [11] and the present approach. First, in the previous case, the projection parameters are derived directly from image line matching. Thus, the recovery of the four affine parameters suffers from the perturbation by the presence of the projective ones. However, in the present case, the recovery of the affine distortion can be completely isolated from the projective one. Thus, the projective distortion has no effect, at least geometrically, on the accuracy of the recovered affine parameters. Secondly, the 1-D mappings depend mainly on intensity values in a region, whereas the contour of the region is used in the present approach.

A further clarification can be made by a comparison between the trace transform [5] and the present approach. First, the trace transform can be used to recover an affine transformation. In contrast, the present approach can be used to recover a general projective transformation. Secondly, the trace transform applies a parallel-beam projection, while the present approach employs a ray projection. Finally, the ideas for evaluating the 1-D functions are similar in both approaches. However, mathematically, the present approach, where only one pair of 1-D functions is employed, is much simpler than the trace transform, where multiple triplets of functions are used.

The rest of this paper is structured as follows. In Section 2, the inverse-polar ray projection for recovering projective transformations between segmented images is presented. Based on the inverse-polar ray projection, a

978-1-4244-2243-2/08/$25.00 ©2008 IEEE

two-step strategy is developed in Section 3 for recovering the eight projective parameters. The experimental results are presented in Section 4. Finally, the conclusions are presented in Section 5, together with some related issues and the future work.

2. Inverse-polar ray projection

2.1. Inverse-polar transform

A two-dimensional (2-D) projective transformation from a point, $\mathbf{x}\left(=[x,y]^T\right)$, in a source image to its counterpart, $\mathbf{x}'\left(=[x',y']^T\right)$, in a target image is:

$$\begin{bmatrix} x' \\ y' \\ 1 \end{bmatrix} = \begin{bmatrix} a & b & g \\ c & d & h \\ e & f & 1 \end{bmatrix} \begin{bmatrix} x \\ y \\ 1 \end{bmatrix}. \tag{1}$$

The projective transformation has eight independent parameters, which are four affine ones, *a*, *b*, *c*, and *d*, two projective ones, *e* and *f*, and two translation-related ones, *g* and *h*, defined as the shift of the target projection center relative to its source counterpart. Much work in motion estimation has focused on finding the translation parameters. Our focus in this work is on recovering the affine and projective parameters.

An image patch can be thought of as a collection of radial line segments from a pole in the patch so that each image point is a point along a 1-D radial line (or ray). A source point on a ray with radial angle θ and radial distance r can be represented as $\mathbf{x}=[r\cos\theta, r\sin\theta]^T$. Similarly, the transformed point can be represented by $\mathbf{x}'=[r'\cos\theta', r'\sin\theta']^T$. Substituting these polar expressions for $\mathbf{x}$ and $\mathbf{x}'$ into Eq. (1), and assuming the two patches have no relative translation, the projective transformation in the inverse-polar space becomes:

$$\begin{cases} \theta' = \tan^{-1}\left(\dfrac{c\cos\theta + d\sin\theta}{a\cos\theta + b\sin\theta}\right), \\ r'_I = \beta(\theta) + \alpha_I(\theta) r_I, \end{cases} \tag{2}$$

where $\alpha_I(\theta)=1/\alpha(\theta)$, $\beta(\theta)=\gamma(\theta)/\alpha(\theta)$, $r_I=1/r$, $r'_I=1/r'$, and two auxiliary parameters, affinely related $\alpha(\theta)$ and projectively related $\gamma(\theta)$, are defined as:

$$\begin{cases} \alpha(\theta) = \sqrt{(a\cos\theta + b\sin\theta)^2 + (c\cos\theta + d\sin\theta)^2}, \\ \gamma(\theta) = e\cos\theta + f\sin\theta. \end{cases} \tag{3}$$

From the second expression in Eq. (2), we see that after converting a source image and its target counterpart from the Cartesian space, I and I', into the inverse-polar space, I_{IP} and I'_{IP}, the projective transformation of a radial line becomes linear. Simple relationships in terms of $\alpha_I(\theta)$ and $\beta(\theta)$ can be established between I_{IP} and I'_{IP} with the help of the ray projection described in the next section.

2.2. Ray projection

A ray projection of an imaged object computes a 1-D functional along each ray crossing the object from a pole. In general, any 1-D (or radial) function, shift-invariant or shift-sensitive, can fit the purpose of the ray projection. In addition, depending on the shape of the object and the location of the pole, a ray projection can cover either a partial angle range ($<2\pi$), forming a fan shape, or the full angle range ($=2\pi$), forming a disc shape. In that sense, the proposed ray projection can be considered as a generalization of the fan-beam projection [6, p. 92] where the radial function is a line integral and the angular span of projection is less than 2π. In the experiments, we illustrate ray projections where the angle range of projection is either less than or equal to 2π.

In the present work, a shift-invariant function and a shift-sensitive function are employed. The former is a line integral as used in the Radon transform [2, p. 505], the fan-beam projection [6, p. 92] and the trace transform [5], while the latter is a ratio of two line integrals as used in the trace transform [5]. For conciseness, the following analysis only takes I'_{IP} as an example. However, all the derived results should be applicable to I_{IP}. Thus, these two functions can be expressed as follows:

Shift-invariant radial function:

$$\text{P: } \int_0^\infty I'_{IP}(r'_I,\theta')\,dr'_I, \tag{4}$$

Shift-sensitive radial function:

$$\text{Q: } \int_0^\infty r'_I I_{IP}(r'_I,\theta)\,dr'_I \Big/ \int_0^\infty I'_{IP}(r'_I,\theta')\,dr'_I. \tag{5}$$

If we directly compute the above functions, we have to first transform an image into the inverse-polar space. Instead, we can evaluate them in the polar space as:

$$\int_0^\infty I'(r',\theta')/r'^2\,dr', \tag{6}$$

$$\int_0^\infty I'(r',\theta')/r'^3\,dr' \Big/ \int_0^\infty I'(r',\theta')/r'^2\,dr'. \tag{7}$$

We can see that the integrands, $I'(r')/r'^2$ and $I'(r')/r'^3$, become infinite at the pole when $I'(0)$ is nonzero. This means that the pole of the ray projection needs to be placed somewhere outside the object.

By applying the ray projection with the above properties to the inverse-polar images, we can solve for the projection parameters.

2.3. Recovery of projective transformation

Based on the inverse-polar ray projection, a two-step approach is developed to recover projective parameters. In

the first step, the affine parameters, *a*, *b*, *c* and *d* are recovered, while in the second step the two projective parameters, *e* and *f*, are recovered.

2.3.1 Recovery of four affine parameters

Before making use of the shift-invariant radial functional properties, we first establish a relationship between two inverse-polar images I_{IP} and I'_{IP}. From the second equation in Eq. (2), this relation can be directly written as:

$$I_{IP}(r_I,\theta) = I'_{IP}(r'_I,\theta') = I'_{IP}(\alpha_I(\theta)r_I + \beta(\theta),\theta'). \quad (8)$$

Then, by applying P to both sides of Eq. (8), we have:

$$\varphi(\theta) = \alpha_I^n(\theta)\varphi'(\theta'), \quad (9)$$

where $\varphi(\theta) = \mathrm{P}(I_{IP}(r_I,\theta))$, $\varphi'(\theta') = \mathrm{P}(I'_{IP}(r'_I,\theta'))$ and $n = -1$.

In order to solve for *a*, *b*, *c* and *d*, we proceed in a two-step normalization of the two angular functions, $\varphi(\theta)$ and $\varphi'(\theta')$. A similar procedure has been proposed in [5] for handling the angular functions derived from the trace transform. The first step normalization reduces the power of $\alpha_I(\theta)$ to one. As a byproduct, $\varphi(\theta)$ and $\varphi'(\theta')$ are normalized. Thus, by raising both sides of Eq. (9) to the power of $1/n$ and rearranging, we obtain:

$$\varphi'_n(\theta') = \alpha(\theta)\varphi_n(\theta), \quad (10)$$

where $\varphi_n(\theta) = \varphi^{1/n}(\theta)$ and $\varphi'_n(\theta) = \varphi'^{1/n}(\theta)$. This states that $\varphi'_n(\theta')$ is the $\varphi_n(\theta)$ scaled by the affine factor $\alpha(\theta)$ defined in Eq. (3). Besides, θ' and θ are affinely related via the first equation in Eq. (2). These two observations illustrate that there exists a 2×2 affine transformation, **A**, with four elements, *a*, *b*, *c* and *d*, between two regions, *R* and R', delimited by $\varphi_n(\theta)$ and $\varphi'_n(\theta')$ [5, 11].

One way to determine **A** is through a normalization of *R* and R'. This second normalization simplifies the relation between *R* and R' from an affinity to a similarity [1, 7]. The related procedure is to construct transformations, $\mathbf{M}^{-1/2}$ and $\mathbf{M}'^{-1/2}$, from the second moment matrices, **M** of *R* and $\mathbf{M}'$ of R', and then to normalize *R* and R' with the derived transformations. It is worth noting that the matrix power, $\mathbf{M}^{-1/2}$ and $\mathbf{M}'^{-1/2}$, can be computed by using an eigenvalue method [3, p. 556].

After the normalization, we obtain two normalized regions delineated by the normalized angular functions, $\varphi_{nM}(\theta_M)$ and $\varphi'_{nM}(\theta'_M)$. As an example, $\varphi_{nM}(\theta_M)$ can be computed from $\varphi_n(\theta)$ via a backward transform technique as follows:

$$\begin{aligned}
&\Delta_{ac} = a_M \sin\theta_M - c_M \cos\theta_M,\\
&\Delta_{db} = d_M \cos\theta_M - b_M \sin\theta_M,\\
&\alpha_M(\theta(\theta_M)) = \det\left(\mathbf{M}^{-1/2}\right) \Big/ \sqrt{\Delta_{ac}^2 + \Delta_{db}^2},\\
&\theta(\theta_M) = \tan^{-1}(\Delta_{ac}/\Delta_{db}),\\
&\varphi_{nM}(\theta_M) = \alpha_M(\theta(\theta_M))\varphi_n(\theta(\theta_M)),
\end{aligned} \quad (11)$$

where a_M, b_M, c_M and d_M are the elements of $\mathbf{M}^{-1/2}$. Similarly, $\varphi'_{nM}(\theta'_M)$ can be computed from $\varphi'_n(\theta')$ as above with $\mathbf{M}'^{-1/2}$ taking over the role of $\mathbf{M}^{-1/2}$.

As mentioned above, there is a similarity transformation, **S**, between $\varphi_{nM}(\theta_M)$ and $\varphi'_{nM}(\theta'_M)$, which can be expressed as follows:

$$\mathbf{S} = \mathbf{M}'^{-1/2}\mathbf{A}\mathbf{M}^{1/2} = s\mathbf{R}$$
$$\text{with } \mathbf{R} = \begin{bmatrix} \cos\theta_{M0} & -\sin\theta_{M0} \\ \sin\theta_{M0} & \cos\theta_{M0} \end{bmatrix}, \quad (12)$$

where *s* is an isotopic scaling (assuming $s > 0$ without loss of generality), and **R** is a rotation by angle θ_{M0}. To determine **S**, we need first to determine θ_{M0} by 1-D mapping $\varphi_{nM}(\theta_M)$ and $\varphi'_{nM}(\theta'_M)$ with the normalized cross-correlation (NCC) as similarity measure. Then, we need to determine *s* as a ratio of the medians of two overlapping segments, $\varphi_{nM}(\theta_M)$ and $\varphi'_{nM}(\theta'_M)$, by which θ_{M0} has been detected with a maximal NCC.

Using Eq. (12), we can compute **S** and, finally, recover the 2×2 affine matrix **A** as:

$$\mathbf{A} = s\mathbf{M}'^{1/2}\mathbf{R}\mathbf{M}^{-1/2}, \quad (13)$$

where $\mathbf{M}'^{1/2}$ and $\mathbf{M}^{-1/2}$ are normalized.

It is worth noting that the above derivation demonstrates mathematically that the affine part of the distortion of an image can be extracted from its general projective one in the inverse-polar space. This unique feature of the inverse-polar ray projection is verified experimentally later.

2.3.2 Recovery of two projective parameters

After determining the four affine parameters, we can recover the two projective parameters, *e* and *f* by invoking the shift-sensitive radial functional properties. In particular, we apply Q to both sides of Eq. (8) and obtain:

$$\psi(\theta) = \alpha_I^n(\theta)(\psi'(\theta') - \beta(\theta)), \quad (14)$$

where $\psi(\theta) = \mathrm{Q}(I_{IP}(r_I,\theta))$ and $\psi'(\theta') = \mathrm{Q}(I'_{IP}(r'_I,\theta'))$. It is worth noting that *n* is always equal to −1 for shift-sensitive functions [5]. Also, since $\alpha_I(\theta) = 1/\alpha(\theta)$ and $\beta(\theta) = \gamma(\theta)/\alpha(\theta)$, we can rewrite the above equation as:

$$\gamma(\theta) = \alpha(\theta)\psi'(\theta') - \psi(\theta). \quad (15)$$

After computing $\alpha(\theta)$ via Eq. (3) and evaluating $\psi(\theta)$ and $\psi'(\theta')$ via the inverse-polar ray projections, we can compute $\gamma(\theta)$ using Eq. (15).

From Eq. (3), we know that $\gamma(\theta)$ contains the two projective parameters, e and f. Thus, to solve for e and f, we need two constraints. Here, we compute e and f as the medians of sequences of e_i and f_i. Each e_i and f_i in the sequences are derived using a pair of values of $\gamma(\theta)$, i.e., $(\gamma(\theta_i), \gamma(\theta_i + \delta_\theta))$, where the two angles, θ_i and $\theta_i + \delta_\theta$, are in the angle range $[\theta_1, \theta_2]$. For $\theta_i + \delta_\theta$ to be in $[\theta_1, \theta_2]$, we need to compute it as an angle modulo the angular span, $\theta_2 - \theta_1$. For simplicity, the angle difference, δ_θ, is kept constant for all pairs.

In particular, two constraints from $(\gamma(\theta_i), \gamma(\theta_i + \delta_\theta))$ can be expressed as:

$$\begin{cases} e\cos\theta_i + f\sin\theta_i = \gamma(\theta_i), \\ e\cos(\theta_i + \delta_\theta) + f\sin(\theta_i + \delta_\theta) = \gamma(\theta_i + \delta_\theta). \end{cases} \quad (16)$$

Solving these linear equations, we obtain e_i and f_i as:

$$\begin{cases} e_i = (\gamma(\theta_i)\sin(\theta_i + \delta_\theta) - \gamma(\theta_i + \delta_\theta)\sin(\theta_i))/\sin(\delta_\theta), \\ f_i = (\gamma(\theta_i + \delta_\theta)\cos(\theta_i) - \gamma(\theta_i)\cos(\theta_i + \delta_\theta))/\sin(\delta_\theta). \end{cases} \quad (17)$$

In the above computation, given one $\gamma(\theta_i)$, we have to choose another, $\gamma(\theta_i + \delta_\theta)$, δ_θ apart. For both $\gamma(\theta_i)$ and $\gamma(\theta_i + \delta_\theta)$ to be able to provide independent information, δ_θ should be as large as possible. On the other hand, to avoid $\sin(\delta_\theta) = 0$ in the above computation, δ_θ cannot be as large as π. Thus, the maximal possible δ_θ equals $\pi/2$, half way between $\gamma(\theta_i)$ and its opposite, $\gamma(\theta_i + \pi)$.

3. Algorithm

Based on the inverse-polar ray projection described above, an algorithm for recovering a projective transformation between two segmented images is outlined below:

(1) Initialization:
- Acquire two segmented image patches, a source image and a target image.
- Set the projection center of the source image patch outside the object.
- Compute $\varphi(\theta)$ for the source image patch with the pole at the projection center according to Eq. (6).
- Determine $\varphi_{nM}(\theta_M)$ by the two-step normalization of $\varphi(\theta)$ according to Eqs. (10) and (11). $\mathbf{M}^{-1/2}$ is also determined.
- Compute $\psi(\theta)$ for the source image patch with the pole at the projection center according to Eq. (7).
- Set a search range for the projection center of the target image patch to, for example, $[-7, 7]$ around a pre-estimated value.

(2) Iterate the following two steps for each point in the search range of the target image patch and update results:

Step 1: Recovering the four affine parameters:
- Compute $\varphi'(\theta')$ along each ray from the projection center of the target image patch according to Eq. (6).
- Determine $\varphi'_{nM}(\theta'_M)$ by the two-step normalization of $\varphi'(\theta')$ according to Eqs. (10) and (11). $\mathbf{M}'^{1/2}$ is also determined.
- Determine θ_{M0} by 1-D mapping $\varphi_{nM}(\theta_M)$ and $\varphi'_{nM}(\theta'_M)$, and set $\mathbf{R}$ according to Eq. (12).
- Determine s as a ratio of the medians of $\varphi_{nM}(\theta_M)$ and $\varphi'_{nM}(\theta'_M)$.
- Recover the affine transformation, $\mathbf{A}$, according to Eq. (13).

Step 2: Recovering the two projective parameters:
- Compute $\psi'(\theta')$ along each ray from the projection center of the target image patch according to Eq. (7).
- Compute $\gamma(\theta)$ according to Eq. (15).
- Compute the two projective parameters, e and f, as medians of sequences e_i and f_i according to Eq. (17).

Update results:

Compute the 2-D similarity (NCC) between the source image patch and the target counterpart and update the records for the recovered projective transformation and the target projection center if NCC is higher.

4. Experimental Results

We experimentally verify that the proposed inverse-polar ray projection can be used to recover a general projective transformation. Our test set consists of: 278×278 "key" (Fig. 1), 202×202 "lock" (Fig. 1), 640×480 "stop sign" (Fig. 6) and 640×480 "fish" (Fig. 6). Transformations between images are either similarity, affine or projective ones. We use global thresholding to segment the object, each of which is less than 150 pixels in each dimension. In two experiments, we use synthetic transformation so that we can compare the recovered parameters with the ground-truth. In these experiments, image warping is performed by the bilinear interpolation.

To show that the angle range of ray projections can vary in $(0, 2\pi]$, the projection centers are placed differently in source images. For image set "key", the

centers are inside the hole, so that the ray projection covers the full angle range. For the other three image sets, the centers are outside the objects. Thus, the related ray projections cover only a partial angle range. However, for comparison, each recovered transformation is presented as if the source projection center were at the center of the source image. In all cases, the ray projection is performed in the polar space with an angular sampling interval 1° and a radial sampling interval 1 pixel.

Recovered transformations are evaluated as follows. First, a recovered transformation is compared with its ground truth if available. Secondly, a similarity measure (NCC) is computed for each pair of matching image patches.

4.1. Recovery of transformations for zoom and rotation

Results from synthetic data. Two synthetic image pairs have been tested. A pair is used to recover the similarity Transformation (1) listed in Table 1; the transformation is a 0.5× digital zoom and a rotation of 60°. The recovered transformation is listed in Table 1 as Transformation (2). We can see that the recovered values are close to their ground truth counterparts. The transformed and reconstructed images are shown in Fig. 2. The obtained 2D similarity measure is 0.963195 for Transformation (2).

The pair is used to check the projective effect on the recovery of a similarity transformation listed in Table 2 as Transformation (3). The recovered transformations are shown in Table 2 as Transformation (4). The recovered values are in a very good agreement with the ground truth. This gives an experimental support to the theoretic analysis that the affine distortion can be separated from a general projective one. The transformed and reconstructed images are shown in Fig. 3. The obtained similarity measure is 0.947707 for Transformation (4).

Results from real data. A real image pair is tested with actual perspective changes captured in the images. The recovered transformations are listed in Table 5 as Transformation (9) and shown in Fig. 7. The obtained 2D similarity measure is 0.965766.

4.2. Recovery of transformations for viewpoint changes

Results from synthetic data. Two synthetic image pairs have been tested. A pair is used to recover the affine transformation (5), listed in Table 3. This transformation is actually extracted from other real image pairs [8]. The recovered transformation is listed in Table 3 as Transformation (6). The transformed and reconstructed images are shown in Fig. 4. The obtained 2D similarity measure is 0.968325.

The other pair is used to check again the projective effect on the recovery of an affine transformation. Transformation (7) in Table 4 adds two new projective parameters. The recovered transformation is listed in Table 4 as Transformation (8). The recovered values are again in a good agreement with the ground truth. This gives a second experimental support to the above analysis that the affine parameters can be determined in the presence of projective distortion. The images are shown in Fig. 5. The similarity measure is 0.954690.

Results from real data. A real image pair is tested with real perspective changes. The recovered transformation is listed in Table 5 as Transformation (10) and shown in Fig. 8. The obtained 2D similarity measure is 0.946382. Our direct experimental results (Table 5) include the detected projection centers of the target image patches. This is because the two translational parameters for a projective transformation can be determined by the shift of the target projection center relative to its source counterpart.

5. Conclusions

The above theoretic analyses and experimental results demonstrate that the proposed inverse-polar ray projection can be used successfully to recover a general projective transformation between two segmented images. In the case where only pure similarity or affine transformations exist between images, the detected values for e and f can, in general, reach as high as an order of 10^{-4}. This phenomenon becomes pronounced when a test object is small. We note that when an object is small, it becomes difficult to obtain a precise description of its boundary. This could be an important factor that affects the accuracy of detected values, especially for the smaller projective parameters.

In our ongoing work, we change the search area for the target projection center from a specified region to a zone surrounding the segmented object. Thus, the recovery of a projective transformation can be carried out automatically. We can also extend the present approach to extract projective-invariant features for an object.

Acknowledgments

This work was supported in part by the Louisiana Governor's Information Technology Initiative.

References

[1] A. Baumberg, "Reliable feature matching across widely separated views," in *Proc. IEEE Conf.*

Computer Vision and Pattern Recognition, Hilton Head Island, SC, pp. 774-781, 2000.

[2] N. R. Bracewell, *Two-Dimensional Imaging*. Prentice Hall, 1995.

[3] G. H. Golub and C. F. Van Loan, *Matrix Computations*, 3rd ed. Johns Hopkins Univ. Press, 1996.

[4] A. Kadyrov and M. Petrou, "The trace transform and its applications," *IEEE Trans. Pattern Analysis and Machine Intelligence*, vol. 23, pp. 811-828, 2001.

[5] A. Kadyrov and M. Petrou, "Affine parameter estimation from the trace transform," *IEEE Trans. Pattern Analysis and Machine Intelligence*, vol. 28, no. 10, pp. 1631-1645, 2006.

[6] A.C. Kak and M. Slaney, *Principles of Computerized Tomographic Imaging*. IEEE Press, 1988.

[7] T. Lindeberg and J. Garding, "Shape-adapted smoothing in estimation of 3-D shape cues from affine deformations of local 2-D brightness structure," *Image & Vision Computing*, vol. 15, pp. 415-434, 1997.

[8] K. Mikolajczyk, T. Tuytelaars, C. Schmid, A. Zisserman, J. Matas, F. Schaffalitzky, T. Kadir, and L. Van Gool, "A comparison of affine region detectors," *Int. J. Comput. Vis.,* vol. 65, pp. 43-72, 2005.

[9] A. B. J. Novikoff, "Integral geometry as a tool in pattern perception: Principles of self organization," in *Trans. Univ. of Illinois Symp. Self-Organization*, H. von Foester and G. Zopf, Jr., eds., London, Pergamon Press, pp. 347-368, 1961.

[10] M. Petrou and A. Kadyrov, "Affine invariant features from the trace transform," *IEEE Trans. Pattern Analysis and Machine Intelligence*, vol. 26, pp. 30-44, 2004.

[11] Y. Zhang and C. H. Chu, "One-dimensional mappings for recovering large scale projective transformations," in *Proc. IEEE Int. Conf. Acoustics, Speech, Signal Processing*, Honolulu, vol. 1, pp. 1021-1024, 2007.

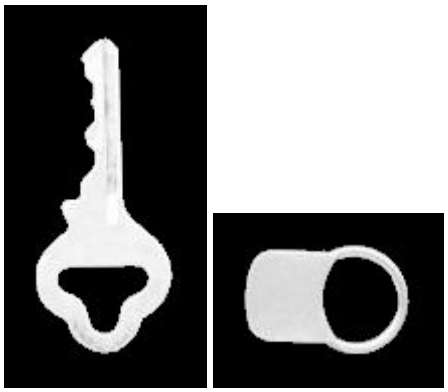

Fig. 1. Original images "key" (*left*) and "lock" (*right*) used in the synthetic transformation experiments.

Table 1. Ground truth and recovered values for image pair with synthetic zoom and rotation.

Transformation Matrix	Center	No.
0.250000 -0.433013 0.000000 0.433013 0.250000 0.000000 0.000000 0.000000 1.000000	139 139	1
0.260945 -0.449556 0.000000 0.428431 0.262142 0.000000 -0.000499 0.000050 1.000000	139.671 138.359	2

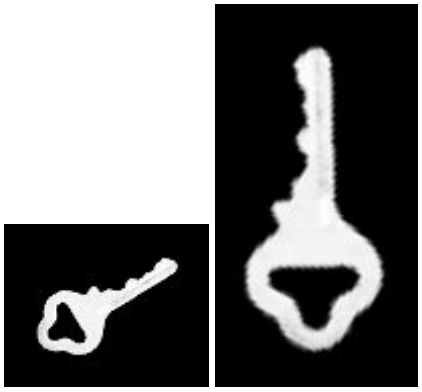

Fig. 2. Image "key" after Transformation (1) (*left*) and reconstructed using recovered Transformation (2) (*right*).

Table 2. Ground truth and recovered values for image pair with synthetic zoom, rotation, and projection.

Transformation Matrix	Center	No.
-0.125000 -0.216506 0.000000 0.216506 -0.125000 0.000000 0.009000 -0.002500 1.000000	139 139	3
-0.145892 -0.210449 0.000000 0.206551 -0.121299 0.000000 0.010876 -0.002359 1.000000	138.638 139.041	4

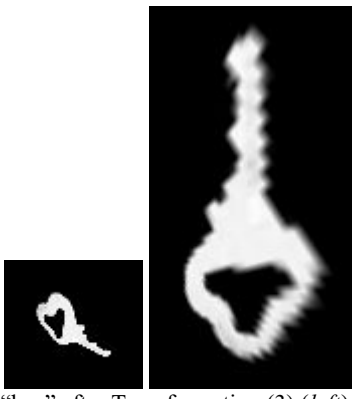

Fig. 3. Image "key" after Transformation (3) (*left*) and reconstructed using recovered Transformation (4) (*right*).

Table 3. Ground truth and recovered values for image pair with synthetic viewpoint change.

Transformation Matrix	Center	No
0.430000 -0.670000 0.000000 0.440000 1.010000 0.000000 0.000000 0.000000 1.000000	101 101	5
0.423208 -0.687868 0.000000 0.438915 1.022944 0.000000 0.000147 -0.000871 1.000000	101.896 99.783	6

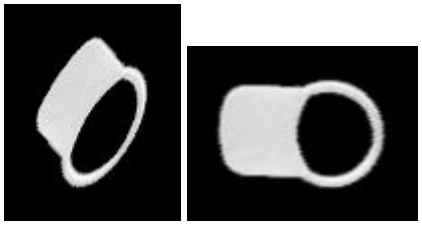

Fig. 4. Image "lock" after Transformation (5) (*left*) and reconstructed using recovered Transformation (6) (*right*).

Table 4. Ground truth and recovered values for image pair with synthetic viewpoint change with perspective effect.

Transformation Matrix	Center	No
0.660000 0.680000 0.000000 -0.150000 0.970000 0.000000 -0.003000 0.009500 1.000000	101 101	7
0.634170 0.739764 0.000000 -0.182782 1.000496 0.000000 -0.003158 0.010456 1.000000	101.443 101.301	8

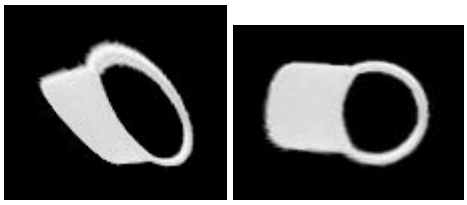

Fig. 5. Image "lock" after Transformation (7) (*left*) and reconstructed using recovered Transformation (8) (*right*).

Table 5. Recovered transformations for real image pairs.

Transformation Matrix	Center	No
0.178730 -0.571547 0.000000 0.576715 0.162475 0.000000 0.000319 0.000389 1.000000	312.833 254.713	9
0.288663 0.618915 0.000000 -0.461713 0.966568 0.000000 -0.000046 -0.000689 1.000000	320.347 229.946	10

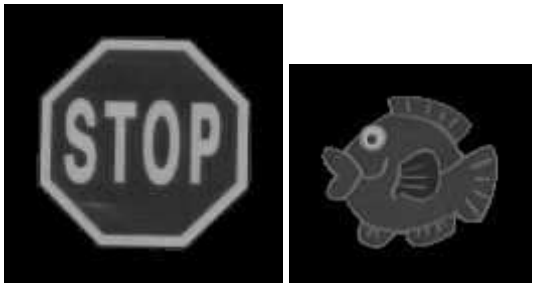

Fig. 6. Original images "stop sign" (*left*) and "fish" (*right*) used in the real transformation experiments.

Fig. 7. Image "stop sign" after zoom and rotation (*left*) and the reconstructed image using recovered Transformation (9) (*right*).

Fig. 8. Image "fish" after transformation due to viewpoint change (*left*) and the reconstructed image recovered Transformation (10) (*right*).